Three-dimensional proton exchange membrane fuel cell model

Carton, James; Olabi, Abdul-Ghani

Published in:
Energy

DOI:
10.1016/j.energy.2016.02.010

Published: 01/10/2017

Document Version
Peer reviewed version

Three-Dimensional Proton Exchange Membrane Fuel Cell Model; Comparison of Double Channel and Open Pore Cellular Foam Flow Plates

J. G. Carton[1*], A. G. Olabi[2]

1. Department of Manufacturing and Mechanical Engineering, Dublin City University, Dublin 9, Ireland.

2. Institute of Engineering and Energy Technologies, University of the West of Scotland, Paisley, PA1 2BE, Scotland

*Email: James.carton3@mail.dcu.ie Phone: +353876328459

ABSTRACT

This study develops a unique three-dimensional computational fluid dynamic electrochemical model for open pore cellular foam material as a flow plate, comparing it to a double channel flow plate and experimental results, researching its application as an alternative to conventional flow plate materials in proton exchange membrane fuel cells.

Using the same membrane electrode assembly and operating parameters, the model simulations, including hydrogen and oxygen distribution and water activity, are examined. IV-curves obtained from the model and experimentally, are analysed and the results are discussed. The model is validated by comparing simulated IV-curve results against experimental results, and model limitations are identified.

The results indicate that the open pore cellular foam material flow plate distributes both hydrogen and oxygen more evenly from inlet to outlet through the fuel cell, when compared to the double channel fuel cell, outperforming it in both simulated and experimental runs.

Keywords: PEM Fuel Cell, Flow Plate, Metal foam, OPCF, RUCS, Electrochemical model.

1 INTRODUCTION

The Proton Exchange Membrane (PEM) fuel cell is a low temperature electrochemical device that offers a promising, possibly green, alternative to traditional power sources, and other fuel cell types, in many applications [1-3].

Simulation results from electrochemical PEM fuel cell models can assist in analysing the chemical reactions within the fuel cell and it aims to gain a more detailed understanding, prediction, control and optimisation of the transport effects, liquid formation and electrochemical activities in PEM fuel cells [4]. The first computational models of PEM fuel cells were recorded in the early 1990s, with most models being one dimensional, isothermal and focusing on the electrode, catalyst layer and membrane [5, 6]. The late 1990's saw the dawn of more advanced and complex PEM fuel cell modelling, 2-D models were first studied and then 3-D models, with multiphase flow following [7]. Single and two phase flow regimes were classified by current density according to the appearance of water at the MEA interface. Extensive research has occurred in the 3-D modelling of PEM fuel cells in recent years. Researchers have modelled many different Gas Diffusion Layer (GDL) materials and thicknesses [8-10] and used various membrane and water models [11, 12], in single phase and multiphase flows [13-15], to optimise fuel cell performance. Researchers have also modelled straight, serpentine and tapered flow plates. Within these models, further researchers have performed analysis of PEM fuel cells, modifying the flow field configurations and even channel rib depth, height and aspect ratio [16-18]. With the aid of models and experimentation results it has been identified that one of the key strategies for improving the performance of the PEM fuel cell is the effective design of the flow plate [19]. By improving the design, layout and configuration of the flow plate with the use of low-cost lightweight construction materials and optimal fabrication methods, the weight, volume and cost of a PEM fuel cell stack can be reduced significantly [20].

Open Pore Cellular Foam (OPCF) materials are an alternative material to machined graphite materials that have been recently used as flow plates [21-25]. OPCF materials have an open pore structure composed of isotropic pores which are connected to each other by ligaments. The array of pores form a solid homogenous matrix, having the same properties of the parent material but at the fraction of the weight. These materials can be manufactured by various processes, casting, foaming, sintering, metal vapor deposition, 3-D printing, etc; according to the size of pore required and state of matter in which the metal is processed [26-28]. A number of researchers, [29-31], have developed computational fluid dynamic models and studied fluid flow, pressure drop and thermal characteristics in different

environments, however none have developed suitable models and electrochemically modelled a fuel cell with a foam flow plate. Developing models and techniques to model these materials is important to further develop fuel cell technology. Carton & Olabi [32] recently developed a Representative Unit Cell Structure (RUCS) model for OPCF material, approximated by a dodecahedron, researching its application as an alternative to conventional PEM fuel cell flow plates. The model gave satisfactory results for pressure drop through the OPCFs, which matched with experimental and mathematical models.

The present study further develops a RUCS, developed by Carton & Olabi, within a 3-D PEM fuel cell electrochemical model. The aim of the study is to compare two PEM fuel cell models; a Double Channel (DCh) flow plate PEM fuel cell with an Open Pore Cellular Foam (OPCF) flow plate PEM fuel cell, both using the same Membrane Electrode Assembly (MEA) and optimised operating parameters.

Simulations are completed on the DCh and OPCF PEM fuel cells and the results are compared against experimental data (polarisation curves obtained experimentally). Effective flow plate design using OPCF flow plate designs are validated and the results are discussed.

2. ELECTROCHEMICAL MODEL DEVELOPMENT

Recently, three-dimensional Computational Fluid Dynamic (CFD) models have been developed by taking full advantage of different commercial CFD software packages such as Fluent, Open-Foam, CFX, Star-CD and CFDRC, etc. The PEM fuel cell module is an extra set of equations, to the normal CFD equations, that have been defined by Fluent Inc., for the modelling of PEM Fuel cells. The Fluent PEM fuel cell module is comprised of several User Defined Functions (UDFs) and a graphical user interface (GUI). The electrochemical reactions occurring on the catalyst are modelled through various source terms while other model parameters are handled through the user interface.

Schematic diagrams of the PEM fuel cell models used in this analysis are illustrated in Figure 1 and Figure 2. Each model consists of cathode and anode gas flow regions, catalyst layers, gas diffusion layers and current collectors (flow plates). In the PEM fuel cell module two electric potential fields are solved. One potential is solved in the membrane and catalyst layers. The other is solved in the

catalyst layers, the diffusion layers and the current collectors. Surface reactions on the porous catalyst region are solved and the reaction diffusion balance is applied to compute the rates. Based on the cell voltage that the user defines, the current density value is computed. Alternatively, a cell voltage can be computed based on a user defined average current density. The liquid water saturation, s, and the water content, λ, are also solved as user-defined scalars [33]. (Refer to the appendix for more detail on the equations defined by Fluent Inc. PEM fuel cell module.) The assumptions made in developing the model are as follows:

- Ideal gas mixtures
- Incompressible and Laminar flow
- Isotropic and homogeneous porous electrodes, catalyst layers and membrane
- Isothermal operation
- Negligible ohmic resistance at porous electrodes and current collectors

The model was imported in to commercial software, Ansys mesh, boundary conditions were added, and it was meshed using either quadrilateral mesh elements or hybrid elements by specifying the minimum edge length. The CFD software version used in this study can only be used with cases containing less than 512,000 elements and so each model has restrictions on its physical dimensions and mesh size. Final models contained between 300,000 and 400,000 elements, course enough not to exceed the limit or computational power or time available, but fine enough to give acceptable results, clarified by grid independence analysis. In this study a grid 20% finer than the base grid was used for a comparison analysis of each mesh. Polarisation curves showed no significant difference in performance of the models; therefore the base mesh was used as it reduced the number of nodes saving computational time.

In order for the CFD analysis software to recognise the PEM fuel cell model, the zone types must be clearly modelled using Ansys Mesh. Two zone types that need to be specified are boundary and continuum zone types. Boundary-type specifications define the physical and operational characteristics of the fuel cell at those topological entities that represent model boundaries. Continuum zone types define the physical characteristics of the model within specified regions of its domain. For the PEM fuel cell module only the cathode and anode collector are specified as the solid

continuum-types, this also simplifies the model [33]. The boundary types are specified as faces while the continuum zone types are the volumes of each component. The boundary zones specified for both the DCh and OPCF electrochemical models are detailed in the Table 1.

With all the zones specified, the mesh was exported ready for analysing. The PEM fuel cell model parameters are set and properties assigned to the relevant regions of the fuel cell before defining the boundary conditions. In order to run the model a minimum number of parameters have to be available to the user; obtained from the fuel cell specifications, experimentation, electrochemistry calculations and existing material properties. A full list of the input parameters for both models is detailed in Table 2 and Table 3. The analysis was carried out at loading conditions of 0.85V (low current density), 0.75V, 0.65V and 0.55V (high current density) and polarisation curves (I-V curve) with a power density curve are plotted. Several key phenomena were monitored during each simulation, until convergence, including continuity and velocity, and checks were made to ensure steady state and low residual RMS error. Flux reports were also analysed; the sum of the flux at the inlet should closely match the flux at the outlet.

2.1 Double Channel Electrochemical Model Development

To reduce complexity and computational demand, a section of the complete double channel flow plate is used for the selected computational domain, see Figure 1.

The domain consists of two, straight, counter flow, channels, each 1mm x 1mm x 37mm. The dimensions of the full domain are 5.5 mm x 5mm x 37mm in the x, y and z directions, respectively. The cross sectional area of the membrane electrode assembly is consequently 192.5mm^2, the area used in obtaining the current density.

The most suitable 3-D mesh for the double channel model is the quad sub-map mesh, which specifies that the mesh includes only quadrilateral mesh elements. This mesh structure is particularly suited for this type of solution because it increases the rate of convergence, increases solution accuracy and reduces the CPU time required.

2.2 Open Pore Cellular Foam Electrochemical Model Development

The 40ppi OPCF flow plate performed satisfactorily in analysis completed by Carton & Olabi [32], and so this model is used in the present study. The 40ppi aluminium foam (ERG Duocel®, US) have the following main characteristics: ligament edge length 0.254mm and pore diameter of 0.635mm. Further information can be found in Table 2 of reference [32] or in reference [34]. To reduce complexity and computational demand, a section of the complete flow plate is used for the selected computational domain, as shown in Figure 2.

The flow plate domain consists of the open pore cellular foam flow plate, 6 pores long by 3 pores wide equating to 2mm x 4mm x 0.62mm. The hydrogen and oxygen are supplied co-flow. The 3-D model is shown in Figure 2 with the hydrogen volume removed, to make the OPCF flow plate visible. The dimensions of the full domain are 2mm x 2.19mm x 4.5mm in the x, y and z directions, respectively. The cross sectional area of the membrane electrode assembly is consequently 9mm^2, this is the area used in obtaining the current density.

The mesh structure was modified to suite this solution and to increases the rate of convergence, reducing the CPU time required, but keeping solution accuracy. The most suitable mesh for the OPCF model is a mixed mesh, which specifies that the mesh includes quadrilateral and tetrahedral mesh elements. The mesh is quiet complex, due to the limitation of 512,000 elements allowed by the software Fluent, and the complexity of OPCF flow plate. This constraint resulted in a physically smaller OPCF model, compared to the DCh model, however all the results were normalised to allow a comparison of both models simulation results.

3 Experimental Set-up

The experimental setup is similar in design to Carton & Olabi [23]. The reactant gas, hydrogen, is stored in a compressed cylinder. A specialised hydrogen pressure regulator (BOC, Ireland) controls the hydrogen gas pressure. Air is provided via a compressor and is regulated with a pressure regulator (SMC, Ireland, with an indicator accuracy of <3% and measured in kPa.). Each gas then passes through a high-precision thermal mass flow meter, calibrated for air or hydrogen gases (Red-y series, Vogtlin Instruments, having an accuracy of 1% and resolution of 0.01ml/min). The flow controllers

are controlled by the data acquisition (DAQ) software (Lab View). An in house humidifier was designed to provide a gas stream at 55°C with between 80-90% humidity. Class 1 K-type thermocouples (Radionics, Ireland with an accuracy of ±1.5°C) were used to measure temperature of the fuel cells. The open circuit voltage and the fuel cell operating voltage are detected by the DAQ hardware and analysed through the software. The open circuit voltage reading is also double checked at the anode and cathode using a multimeter. The fuel cell current is measured using a multimeter in series with the external load. The meter used to measure current and voltage from the fuel cells (Fluke 8808A digital multimeter) has 0.01% accuracy and 10uV resolution.

The experimental DCh and OPCF fuel cell used the same MEA and same operating parameters, see Table 4 and Table 5. Every effort was made to keep parameters constant during the experiments to ensure that the values of temperature, pressure and flow were not changed from one experiment to the next. These parameters were checked throughout the experiment to identify any unwanted errors. To ensure statistically correct results experiments were repeated for each fuel cell at least 3 times in order to present the average I-V curve result, as shown in Figure 8. The only effect on the performance was that of the flow plate design.

4 RESULTS & DISCUSSION

As discussed in section 2, due to constraints of the software, the OPCF model is smaller compared to the DCh model. To view the results clearly planes (surfaces) are created through different parts of each model (the velocity profile is shown in Figure 3 for example). The planes allow for a 2-D view of the results for easier comparison. All results presented below are representing the fuel cell operating at 0.55V (high current density).

4.1 Fluid Velocity Flow

Figure 3 shows the velocity profile results through both the DCh and OPCF PEM fuel cells. The velocity flow in the DCh PEM fuel cell, Figure 3 (a), is even with minimal convective flow along the straight, long channels in this flow plate configuration.

In contrast, the velocity flow in the OPCF PEM fuel cell, Figure 3 (b), is more disrupted with convective flow, and regions of medium velocity and high velocity noticed along this flow plate configuration.

4.2 Hydrogen and oxygen distribution

The hydrogen mass fraction, as shown in Figure 4, decreases in the direction of flow, due to the hydrogen being consumed in the fuel cell, and by the transport of water from the anode to the cathode, due to osmotic drag. The DCh PEM fuel cell, enlarged to a suitable scale in Figure 4 (b), shows a sharper decrease in hydrogen compared to the OPCF PEM fuel cell, Figure 4 (c), which can be attributed to the OPCF flow plate allowing the hydrogen to be distributed over its entire active area rather than just in the channel areas. Figure 4 (d) shows a plot of hydrogen and oxygen distribution in the anode and cathode along each fuel cell. The oxygen mass fraction is seen to decrease gradually and consistently in both simulated PEM fuel cells as it is consumed. This seemingly slow decrease is related to the mass fraction of oxygen compared to its mixture, of water produced (during the reaction) and the nitrogen in the air.

The concentration of hydrogen at the anode in both simulated PEM fuel cells is evenly distributed throughout the flow plate voids, showing only one colour (graphs not shown), with negligible differences of hydrogen even within the channels or within the GDL. However, looking at section profiles in corresponding points of both PEM fuel cells in Figure 5, the oxygen concentration can be viewed. The concentration of oxygen in the DCh PEM fuel cell, Figure 5 (a) (magnified section) shows even distribution of oxygen within the channel, however it shows reduced concentrations under the ribs of the channels.

In conventional flow plate designs (including DCh as presented) a large area of the GDL is covered by the channel, affecting fluid and gas flow through the fuel cell and GDL, noted by researchers such by Dohle et al. [35] as an important area to consider when designing fuel cells. In contrast to this effect, the OPCF PEM fuel cell, Figure 5 (b), shows an even concentration throughout the flow region. This even distribution can be attributed to the open matrix structure of the OPCF material.

4.3 Water distribution

The properties of the MEA dictate the level of humidity required in the gas flow and as stated by the manufacturer of the membrane (DuPont, US) and the supplier of the MEA (Fuel Cell Store, US) the MEA should be fully humidified. Water is introduced in the gas flow to keep the polymer electrolyte active and compensate for water losses due to the electro-osmotic action in the electrolyte. Many researches have shown that water production, especially at high current densities can lead to water flooding issues in PEM channels [36-38]. In other studies researchers have modelled, observed and visualised water droplet formation and flooding [39-43].

The model used in this study does not take into account the phase change and two-phase flow of the water through the channels; therefore these results only show the liquid water activity within the cell. However the indication of the existence of the liquid water in the catalyst and the gas diffusion layers is important as water can block the effective reacting surface and the pores of the diffusion layer, causing flooding.

The predicted water transportation along the DCh and OPCF fuel cells anodes and the cathodes are presented in Figure 6, with an end, or through plane, view of the anode and cathode shown in Figure 7.

In the DCh fuel cell, Figure 6 (a), on the anode side (upper channel) the water concentration steadily increases along the gas flow, from inlet to outlet. This can be associated to back diffusion from the cathode which is sufficient to counteract the electro-osmotic drag.

In the DCh fuel cell cathode (lower channel), the content of water increases slowly then stabilises before it drops slightly almost matching the anode side. Figure 6(c) shows a clearer view the water distribution in the anode and cathode flow channels. Under high current density the electro-osmotic effect can dominate back diffusion. These phenomena can result in a drier anode as seen with the slight decrease of water toward the end of the channel in the anode.

In Figure 7 (a) the results indicate there are increased concentrations of water under the ribs of the DCh fuel cell, potentially leading to localised flooding issues. This could explain how flooding can hinder the oxygen reduction reaction in conventional flow plate designs.

The OPCF fuel cell results indicate that water is more evenly distributed in the entire domain, as shown in Figure 7 (b). Water production is seen to increase in the anode, however high concentrations of water are not detected, indicating that flooding issues may be reduced.

4.4 DCh & OPCF electrochemical simulation results comparison

The flow field profile is very important in conventional flow plates such as serpentine; the flow is in the direction parallel to the electrode surface. In this configuration the reactant flow to the catalyst layer is predominantly by molecular diffusion through the GDL. This can lead to large concentration gradients across the GDL and mass transfer limitations, because of the small channel dimensions, laminar gas flow and the inherent slow molecular diffusion process [44].

Due to the matrix of ligaments and pores in OPCF flow plates, the flow travels a more tortuous path through the flow field making the flow of reactant gases towards the reaction interface from only diffusion to diffusion plus convection based, unlike conventional flow plates. This can provide for better mass transfer and potentially enhanced water removal from the GDL, which was also noticed by Carton & Olabi [32], when they modelled pressure drop through OPCFs.

In existing flow fields, intricate flow field structures are common but on a much larger scale when compared to OPCF materials, which have sub millimetre pores and ligaments to distribute the flow. It is noted that permeability reduction with the conventional machined channel design is not possible beyond a particular value (around 10^{-8} m^2), due to difficulty in machining thin cross-section channels [19]. This is not an issue for OPCF materials, with a measured permeability of $10^{-8}m^2$, for 40ppi foam for example and with the added benefit of low pressure drop from inlet to outlet, even at high flow rates.

Owing to the excellent conductivity of a metal OPCF the OPCF fuel cell model exhibited better current density results when compared to the double channel model (graphs not shown). The concentration of current is mainly on the GDL and incorporates the full area under the flow plate. Similarly the OPCF fuel cell model showed an even spread of temperature throughout the cell, indicating a better distribution of heat in the open structure flow plate compared to the DCh fuel cell.

The design of the flow plate with OPCF material has good surface contact of the ligaments with the GDL, open structure, and excellent gas diffusion allowing for uniform current and gas distribution, low ohmic internal resistance and high rates of mass transport of the electro active species to the electrode surface. This provides enhanced performance at high current density operation.

The characteristic polarisation or I-V curve with an integrated power density curve is used extensively to measure the performance of a PEM fuel cell. The double channel (DCh) and open pore cellular foam (OPCF) flow plates were tested to ensure a consistent bench mark against the development electrochemistry models. PEM fuel cell simulation and experimental results for DCh and OPCF flow plates as shown in Figure 8.

The polarisation curve of any fuel cell can be divided into three sections where each section is dominated by a different type of voltage loss mechanism, The first region which is dominated by a sharp decline in voltage is associated to activation loss, which is a result of slow reaction kinetics related to the type of catalyst used, oxygen concentration and cell temperature. Since all these parameters were constant in the study both DCh and OPCF fuel cells have similar losses in this region, as shown in Figure 8. The next region is recognised by a straight sloping decrease of voltage, associated with ohmic losses, related to electrical and proton loss. The OPCF fuel cell performs better compared to the DCh fuel cell. With the same membrane used in both fuel cells the improved performance is associated to the metal OPCF, compared to the graphite DCh flow plates. From figure 8 the main difference viewed is in the final region. During experimentation the DCh fuel cell did not perform as well below 0.55V, with the voltage decreasing rapidly and the current density increasing slowly. This region is related to the mass transport limitation of the fuel cell. The loss is particularly associated with the cathode side where not enough oxygen reaches the active sites of the catalyst layer. In addition reactive sites or the GDL can become blocked, at high current densities, due to excessive water production that is not moved. The OPCF fuel cell performed continuously to below 0.5V with no drop off due to mass transport limitation. The polarisation curves constructed match experimental results well, however the model did not accurately predict mass transport limitations of

the DCh fuel cell, mainly due to the limitation of the Fluent fuel cell module used in this study, which does not take into account the phase change and two-phase flow of the water through the channels.

However, from both experimental and simulated results the OPCF flow plate outperformed the conventional flow plate, recording 0.7V at 0.09A/cm^2. This is in excess of a 55% improvement on the current density of the bench mark DCh flow plate under the same operating conditions operating at 0.7 volts.

4. CONCLUSION

This paper developed a unique three-dimensional Open Pore Cellular Foam (OPCF) PEM fuel cell electrochemical model using a Representative Unit Cell Structure (RUCS) model for OPCF material, comparing it to a Double Channel (DCh) PEM fuel cell model and experimental results, using the same Membrane Electrode Assembly (MEA) and operating parameters. The model is validated by comparing simulated IV-curve results against experimental results, and model limitations are identified. For the presented DCh and OPCF PEM fuel cell models reasonable predictions have been obtained and discussed. The conclusions resulting from the investigation are summarised as follows:

- Hydrogen and oxygen were distributed more evenly from inlet to outlet of the OPCF flow plate, when compared to the DCh model.
- The model results indicated that the OPCF flow plates managed temperature and water in the PEM fuel cell better than the DCh model.
- Mass transport limitations were reduced in the OPCF fuel cell compared to the Dch fuel cell.
- The OPCF flow plate outperformed the conventional flow plate, recording 0.7V at 0.09A/cm^2.

The advantages of the OPCF flow plates have huge implications on flood mitigation, mass transport losses reduction, and increasing the PEM fuel cell performance. Future work could focus on using this work, in conjunction with experiments performed by other groups such as Chen [45] to study the hydration effects on the membrane activity using foam flow plates.

List of Acronyms

MEA Membrane Electrode Assembly

PEM Proton Exchange Membrane

GDL Gas Diffusion Layer

OPCF Open Pore Cellular Foam

RUCS Representative Unit Cell Structure

MF Metal Foam

CFD Computational Fluid Dynamic

UDF User-Defined Function

Pt Platinum

DCh Double Channel

Sim Simulation

Exp Experimental

3-D Three Dimensional

O2 Oxygen

H2 Hydrogen

Appendix

Appendix A - Electrochemical Modelling

The following is a description of the useful electrochemical equations defined by Fluent Inc. in the PEM fuel cell module, for a full review of these equations the reader is referred to [33].

At the centre of the electrochemistry is the computation of the rate of the hydrogen oxidation and the rate of oxygen reduction. These electrochemical processes are treated as heterogeneous reactions that take place on the catalyst surfaces inside the two catalyst layers on both sides of the membrane. The driving force behind these reactions is the surface over-potential, the difference between the phase potential of the solid and the phase potential of the electrolyte/membrane.

Two potential equations are first solved for in the PEM model:

$$\Delta(\sigma_{sol}\,\phi_{sol}) + R_{sol} = 0 \qquad \textit{Eqn. (1)}$$

accounts for the electron transport e^- through the solid conductive materials and:

$$\Delta(\sigma_{mem}\,\phi_{mem}) + R_{mem} = 0 \qquad \textit{Eqn. (2)}$$

represents the protonic transport of H^+ where σ is the electrical conductivity (1/ohm-m), ϕ is the electric potential (volts) and R is the volumetric transfer current (A/m^3). External boundary conditions must be added to the model to solve for ϕ_{sol} and ϕ_{mem}.

The source terms in Equations (1) and (2) are also called the exchange current density (A/m^3), and have the following general definitions:

$$R_{an} = j_{refan}\,([H_2]/([H_2]_{ref})^{\gamma an}\,(e^{\alpha anF\eta an/RT} - e^{-\alpha catF\eta an/RT}) \qquad \textit{Eqn. (3)}$$

$$R_{cat} = j_{refcat}\,([O_2]/([O_2]_{ref})^{\gamma cat}\,(-e^{+\alpha anF\eta cat/RT} + e^{-\alpha catF\eta cat/RT}) \qquad \textit{Eqn. (4)}$$

where j^{ref} is the volumetric reference exchange current density (A/m^3), [O2] & [H2] are the local species concentration, reference value ($kgmol/m^3$), γ is the concentration dependence, α is the transfer coefficient and F is the Faraday constant. The above equation is the general formulation of the Butler-Volmer function. A simplification to this is the Tafel formulation that reads:

$$R_{an} = j_{refan}\,([H_2]/([H_2]_{ref})^{\gamma an}\,(e^{\alpha anF\eta an/RT}) \qquad \textit{Eqn. (5)}$$

$$R_{cat} = j_{refcat}\,([O_2]/([O_2]_{ref})^{\gamma cat}\,(e^{-\alpha catF\eta cat/RT}) \qquad \textit{Eqn. (6)}$$

By default, the Butler-Volmer function is used in the Fluent PEM fuel cell model to compute the transfer currents inside the catalyst layers. The driving force for the kinetics is the local surface over-potential, η, also known as the activation loss. It is generally the difference between the solid and membrane potentials, ϕ_{sol} and ϕ_{mem}. The gain in electrical potential from crossing from the anode to the cathode side can then be taken into account by subtracting the open-circuit voltage V_{oc} on the cathode side:

$$\eta_{an} = \sigma_{sol} - \phi_{mem} \qquad \textit{Eqn. (7)}$$

$$\eta_{cat} = \sigma_{sol} - \phi_{mem} - V_{oc} \qquad \textit{Eqn. (8)}$$

From these equations the two potential fields can be obtained.

Current and mass conservation

The following reactions occur, respectively, at the anode and the cathode:

$$H_2 = 2H^+ + 2e^- \qquad \textit{Eqn. (9)}$$

$$O_2 + 4H^+ + 4e^- = 2H_2O \qquad \textit{Eqn. (10)}$$

The volumetric source terms for the species equations (kg/m^3-s) and energy equation (W/m^3) are given as:

$$SH_2 = (-M_{w,}H_2/2F)R_{an} \qquad \textit{Eqn. (11)}$$

$$SO_2 = (-M_{w,}O_2/4F)R_{cat} \qquad \textit{Eqn. (12)}$$

$$SH_2O = (M_{w,}H_2O/2F)R_{cat} \qquad \textit{Eqn. (13)}$$

Additional volumetric sources to the energy equation implemented in the Fluent PEM model include ohmic heating, heat of formation of water, electric work and latent heat of water.

$$S_h = I^2R_{ohm} + h_{reaction} + \eta R_{an,cat} + h_{phase} \qquad \textit{Eqn. (14)}$$

The species concentrations of hydrogen and oxygen in the rate calculation are the surface values, and it is assumed that the diffusive flux of any reacting species is balanced by its rate of production.

$$\rho D_i / \delta(y_{i,surf} - y_{i,cent})r = M_{w,i}/\eta F)\, R_{an,cat} \qquad \textit{Eqn. (15)}$$

where D_i is the mass diffusivity of species i (m^2/s), r is the specific reacting surface area of the catalyst layer or surface-to-volume ratio (1/m), $y_{i,surf}$ is the mass fraction of species *i* at the reacting

surface, $y_{i,cent}$ is the mass fraction of species *i* at the cell centre, $\delta = 1/r$ is the average distance between the reaction surfaces and the cell centre (m). The left hand side of this equation represents the diffusive flux at the reacting surface and the right hand side represents the rate of mass generation. This equation can be used to obtain the surface values of H_2 and O_2 concentrations, applying a Newtonian solution procedure. These surface, or wall, values are then used to compute the rates in Equation (11) through to Equation (13).

Liquid water formation, transport & effects

PEM fuel cells operate less than one hundred degrees Celsius and water vapour may condense to liquid water, especially at high current densities. To model the formation and transport of liquid water, including various physical processes such as condensation, vaporization, capillary diffusion, and surface tension, Fluent PEM model uses a saturation model. In this approach, the liquid water formation and transport is governed by a conservation equation for the volume fraction of liquid water, s, or the water saturation:

$$\delta(\varepsilon \rho s / \delta t) + \nabla . (\rho V s / \delta t) = r_w \qquad \textit{Eqn. (16)}$$

where r_w is the condensation rate.

The electrolyte membrane of the fuel cell is modelled as a porous fluid zone. Properties such as membrane phase electrical conductivity, osmotic drag coefficient, back diffusion flux and membrane water diffusivity are evaluated as functions of the water content, λ.

$$\lambda = 14 + 1.4 (\alpha - 1) \; (\alpha > 1) \qquad \textit{Eqn. (17)}$$

where α is the water activity that is calculated from the water vapour pressure and saturation pressure of water.

Accounting for advection and diffusion in the PEM fuel cell

It is important to also have a basic understanding of species transport and how CFD accounts and calculates specie concentrations. A basic concept for the movement of species is that a specie within a gas volume will tend to spread evenly within the gas. When a higher quantity of a specie is located in one part of the volume than another, a potential is generated measured by the partial pressure of the

specie. This potential drives some of the specie at the higher concentration into the zone where the species is at a lower concentration. This is referred to as pure diffusion mass transfer. In reality this may also occur in a fluid in motion and then the diffusion potential must be combined with the forces causing the fluid to move which will aid or hinder the diffusion of the species and this is referred to as advection. A similar equation to Equation (21) may be derived for any physical quantity that is advected or diffused by a fluid flow. For each such quantity an equation is solved for the concentration (i.e. amount per unit mass), for example, the concentration of salt, sediment or chemical constituent. Diffusion occurs when concentration varies with position. It typically involves transport from regions of high concentration to regions of low concentration, at a rate proportional to area and concentration gradient. For many scalars it may be quantified by Fick's diffusion law as seen below:

$$rate\ of\ diffusion = -\ diffusivity\ x\ gradient\ x\ area \qquad Eqn.\ (18)$$

or

$$rate\ \ of\ \ \ diffusion = -\Gamma \times \frac{\partial \phi}{\partial n} \times A \qquad Eqn.\ (19)$$

Equation 19 is often referred to as gradient diffusion. A common example is heat conduction or in the case of fuel cells partial pressure gradients in the oxidant and fuel channels. For an arbitrary control volume the mass of specie inside a PEM fuel cell can be described as the mass inside the cell multiplied by the concentration inside:

$$Amount\ in\ cell = \rho\ x\ V\ x\ \phi \qquad Eqn.\ (20)$$

The advective flux of a specie inside a PEM fuel cell can be described by multiplying the mass flux by the concentration of the specie:

$$Advective\ flux = C\ x\ \phi \qquad Eqn.\ (21)$$

The diffusive flux of a specie inside a PEM fuel cell can be described by the diffusivity of the specie in the mixture times the gradient of the concentration of the specie within the mixture multiplied by an area as seen in Equation 22:

$$Diffusive\ \ flux = -\Gamma \times \frac{\partial \phi}{\partial n} \times A \qquad Eqn.\ (22)$$

The quantity of a species produced or removed in a PEM fuel cell can be determined by multiplying the source/sink density by the volume as seen in Equation 23:

$$Source = S \times V \qquad \textit{Eqn. (23)}$$

Balancing the rate of change against the net flux through the boundary and rate of production yields the scalar-transport or (advection-diffusion). Please refer [33] for further information.

Porous jump boundary conditions

Porous jump conditions are used to model a thin "membrane" that has known velocity (pressure-drop) characteristics. It is essentially a 1-D simplification of the porous media model available for cell zones. This simpler model is used whenever possible, instead of the full porous media model, because it is more robust and yields better convergence. The thin porous medium has a finite thickness over which the pressure change is defined as a combination of Darcy's Law and an additional inertial loss term:

$$\Delta p = -(\mu/\alpha\, v + 0.5 C_2 \rho v^2)\Delta m \qquad \textit{Eqn. (24)}$$

where μ is the laminar fluid viscosity, α is the permeability of the medium, C_2 is the pressure-jump coefficient, v is the velocity normal to the porous face, and Δm is the thickness of the medium. Appropriate values for α and C_2 can be calculated using the techniques described in [33].

REFERENCES

[1]Carton JG, Olabi AG. Wind/hydrogen hybrid systems: Opportunity for Ireland's wind resource to provide consistent sustainable energy supply. Energy 2010;35(12):4536-4544.

[2]Achour H, Carton JG, Olabi AG. Estimating vehicle emissions from road transport, case study: Dublin City. Applied Energy 2011;88(5):1957-1964.

[3]Lawlor V, Zauner G, Hochenauer C, Mariani A, Griesser S, Carton JG, et al. The Use of a High Temperature Wind Tunnel for MT-SOFC Testing-Part I: Detailed Experimental Temperature Measurement of an MT-SOFC Using an Avant-Garde High Temperature Wind Tunnel and Various Measurement Techniques. Journal of Fuel Cell Science and Technology 2010 12;7(6):061016 (7 pp.).

[4]Djilali N. Computational modelling of polymer electrolyte membrane (PEM) fuel cells: Challenges and opportunities. Energy 2007 04;32(4):269-80.

[5]Bernardi DM, Verbrugge MW. Mathematical model of a gas diffusion electrode bonded to a polymer electrolyte. AICHE J. 1991;37(8):1151-1163.

[6]Bernardi DM, Verbrugge MW. A mathematical model of the solid-polymer-electrolyte fuel cell. J.Electrochem.Soc. 1992;139(9):2477-91.

[7]Wang ZH, Wang CY, Chen KS. Two-phase flow and transport in the air cathode of proton exchange membrane fuel cells. J.Power Sources 2001 02/15;94(1):40-50.

[8]Zhou T, Liu H. Effects of the electrical resistances of the GDL in a PEM fuel cell. J.Power Sources 2006 10/20;161(1):444-453.

[9]Kopanidis A, Theodorakakos A, Gavaises M, Bouris D. Pore scale 3D modelling of heat and mass transfer in the gas diffusion layer and cathode channel of a PEM fuel cell. International Journal of Thermal Sciences 2011 4;50(4):456-467.

[10]Taymaz I, Benli M. Numerical study of assembly pressure effect on the performance of proton exchange membrane fuel cell. Energy 2010 5;35(5):2134-2140.

[11]Karpenko-Jereb L, Innerwinkler P, Kelterer A-, Sternig C, Fink C, Prenninger P, et al. A novel membrane transport model for polymer electrolyte fuel cell simulations. Int J Hydrogen Energy 2014 4/24;39(13):7077-7088.

[12]Dawes JE, Hanspal NS, Family OA, Turan A. Three-dimensional CFD modelling of PEM fuel cells: An investigation into the effects of water flooding. Chemical Engineering Science 2009 6/15;64(12):2781-2794.

[13]T. Berning, D. M. Lu and N. Djilali. Three-dimensional computational analysis of transport phenomena in a PEM fuel cell. Anonymous 7th Grove Fuel Cell Symposium, Grove VII, September 11, 2001 - September 13106 London, United kingdom: Elsevier; 2001; 284-294.

[14]Gurau V, Zawodzinski Jr. TA, Mann Jr. JA. Two-phase transport in PEM fuel cell cathodes. Journal of Fuel Cell Science and Technology 2008;5(2).

[15]Gurau V, Mann JA. A critical overview of computational fluid dynamics multiphase models for proton exchange membrane fuel cells. SIAM J Appl Math 2009;70(2):410-454.

[16]Ferng YM, Su A. A three-dimensional full-cell CFD model used to investigate the effects of different flow channel designs on PEMFC performance. Int J Hydrogen Energy 2007 12;32(17):4466-4476.

[17]Manso AP, Marzo FF, Mujika MG, Barranco J, Lorenzo A. Numerical analysis of the influence of the channel cross-section aspect ratio on the performance of a PEM fuel cell with serpentine flow field design. Int J Hydrogen Energy 2011 6;36(11):6795-6808.

[18]Hashemi F, Rowshanzamir S, Rezakazemi M. CFD simulation of PEM fuel cell performance: Effect of straight and serpentine flow fields. Math.Comput.Model. 2012 2;55(3–4):1540-1557.

[19]Kumar A, Reddy RG. Materials and design development for bipolar/end plates in fuel cells. Journal of Power Sources 2004;129(1):62-67.

[20]Steele BCH, Heinzel A. Materials for fuel-cell technologies. Nature 2001;414(6861):345-352.

[21]Ashby MF, Evans AG, Fleck NA, Gibson LJ, Hutchinson JW, Wadley HNG. Metal Foams: A design Guide. 1st ed. Massachusetts: Butterworth-Heinemann; 2000.

[22]Friedrich JM, Ponce-de-Leon C, Reade GW, Walsh FC. Reticulated vitreous carbon as an electrode material. J Electroanal Chem 2004;561(1-2):203-217.

[23]Watkins D, Dircks K, Epp D, inventors. Watkins D, Dircks K and Epp D, assignees. Fuel cell with a fluid flow field plate. EU patent 04157331991.

[24]OLABI AG, CARTON JG, inventors. Dublin City University, assignee. A proton exchange membrane fuel cell with open pore cellular foam. Ireland patent WO2014037494.

[25]Watkins D, Dircks K, Epp D, inventors. Watkins D, Dircks K and Epp D, assignees. Fuel cell fluid flow field plate. US patent 51088491992.

[26]Girlich D. Open Pore Metal Foam. 2008; Available at: http://www.m-pore.de/Download/CellMet-Veroeffentlichung_4_.pdf.

[27]Banhart J. Manufacture, characterisation and application of cellular metals and metal foams. Progress in Materials Science 2001;46(6):559-632.

[28]Parvanian AM, Panjepour M. Mechanical behavior improvement of open-pore copper foams synthesized through space holder technique. Mater Des 2013 8;49(0):834-841.

[29]Du Plessis P, Montillet A, Comiti J, Legrand J. Pressure drop prediction for flow through high porosity metallic foams. Chemical Engineering Science 1994;49(21):3545-3553.

[30]Krishnan S, Murthy JY, Garimella SV. Direct simulation of transport in open-cell metal foam. Journal of Heat Transfer 2006;128(8):793-799.

[31]Shankar Krishnan, Suresh V. Garimella and Jayathi Y. Murthy. Simulation of thermal transport in open-cell metal foams: Effect of periodic unit cell structure. Anonymous International Mechanical Engineering Congress and Exposition, IMECE2006, November 5 -November 10 Chicago, IL, United states: American Society of Mechanical Engineers; 2006; .

[32]Carton JG, Olabi AG. Representative model and flow characteristics of open pore cellular foam and potential use in proton exchange membrane fuel cells. Int J Hydrogen Energy 2015 5/4;40(16):5726-5738.

[33]Fluent Inc. Fluent Manual & Theory Guide. U.S.,2010. See Also: Accessed through: www.ansys.com.

[34]ERG Materials and Aerospace Corp. Material Specific Properties of Metal Foam. US, 2009. See Also: http://www.ergaerospace.com/.

[35]Dohle H, Jung R, Kimiaie N, Mergel J, Muller M. Interaction between the diffusion layer and the flow field of polymer electrolyte fuel cells - Experiments and simulation studies. J.Power Sources 2003;124(2):371-384.

[36]Quan P, Ming-Chia Lai. Numerical study of water management in the air flow channel of a PEM fuel cell cathode. J.Power Sources 2007;164(1):222-37.

[37]Zhou B, Quan P, Sobiesiak A, Liu Z. Water behavior in serpentine micro-channel for proton exchange membrane fuel cell cathode. J.Power Sources 2005 12/01;152:131-45.

[38]Zhu X, Sui PC, Djilali N. Dynamic behaviour of liquid water emerging from a GDL pore into a PEMFC gas flow channel. J.Power Sources 2007;172(1):287-295.

[39]Jay Benziger, Tamara Whitaker, Erin Kimball and I. G. Kevrekidis. Liquid water transport in PEM fuel cells. Anonymous Fuel Cell Seminar 2007, October 15, 2007 - October 1912 San Antonio, TX, United states: Electrochemical Society Inc; 2007; 67-79.

[40]Erin Kimball, Tamara Whitaker, I. G. Kevrekidis and J. B. Benziger. Drops, slugs and flooding in PEM fuel cells. Anonymous 7th Symposium Devoted to Proton Exchange Membrane Fuel Cells - 212th ECS Meeting, October 7, 2007 - October 1211 Washington, DC, United states: Electrochemical Society Inc; 2007; 725-736.

[41]Bazylak A. Liquid water visualization in PEM fuel cells: a review. Int J Hydrogen Energy 2009 05;34(9):3845-57.

[42]Bazylak A, Heinrich J, Djilali N, Sinton D. Liquid water transport between graphite paper and a solid surface. J.Power Sources 2008;185(2):1147-1153.

[43]Carton JG, Lawlor V, Olabi AG, Hochenauer C, Zauner G. Water droplet accumulation and motion in PEM (Proton Exchange Membrane) fuel cell mini-channels. Energy 2012;39(1):63-73.

[44]Kazim A, Liu HT, Forges P. Modelling of performance of PEM fuel cells with conventional and interdigitated flow fields. J.Appl.Electrochem. 1999 12;29(12):1409-16.

[45] Chen, J. Experimental study on the two phase flow behavior in PEM fuel cell parallel channels with porous media inserts, J.Power Sources,2010; 195(4): 1122-1129.

Figure 1
Click here to download high resolution image

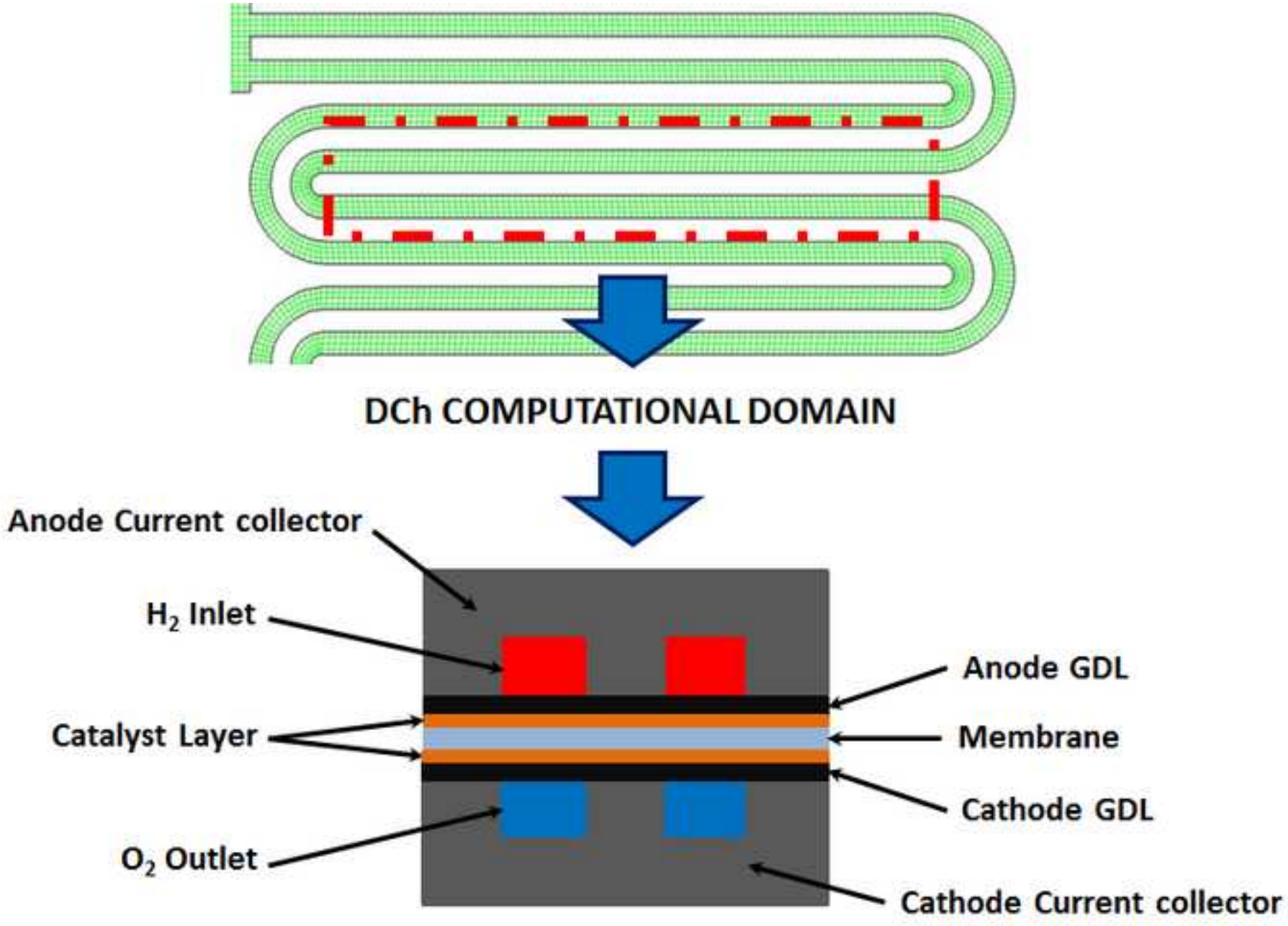

Figure 2

Click here to download high resolution image

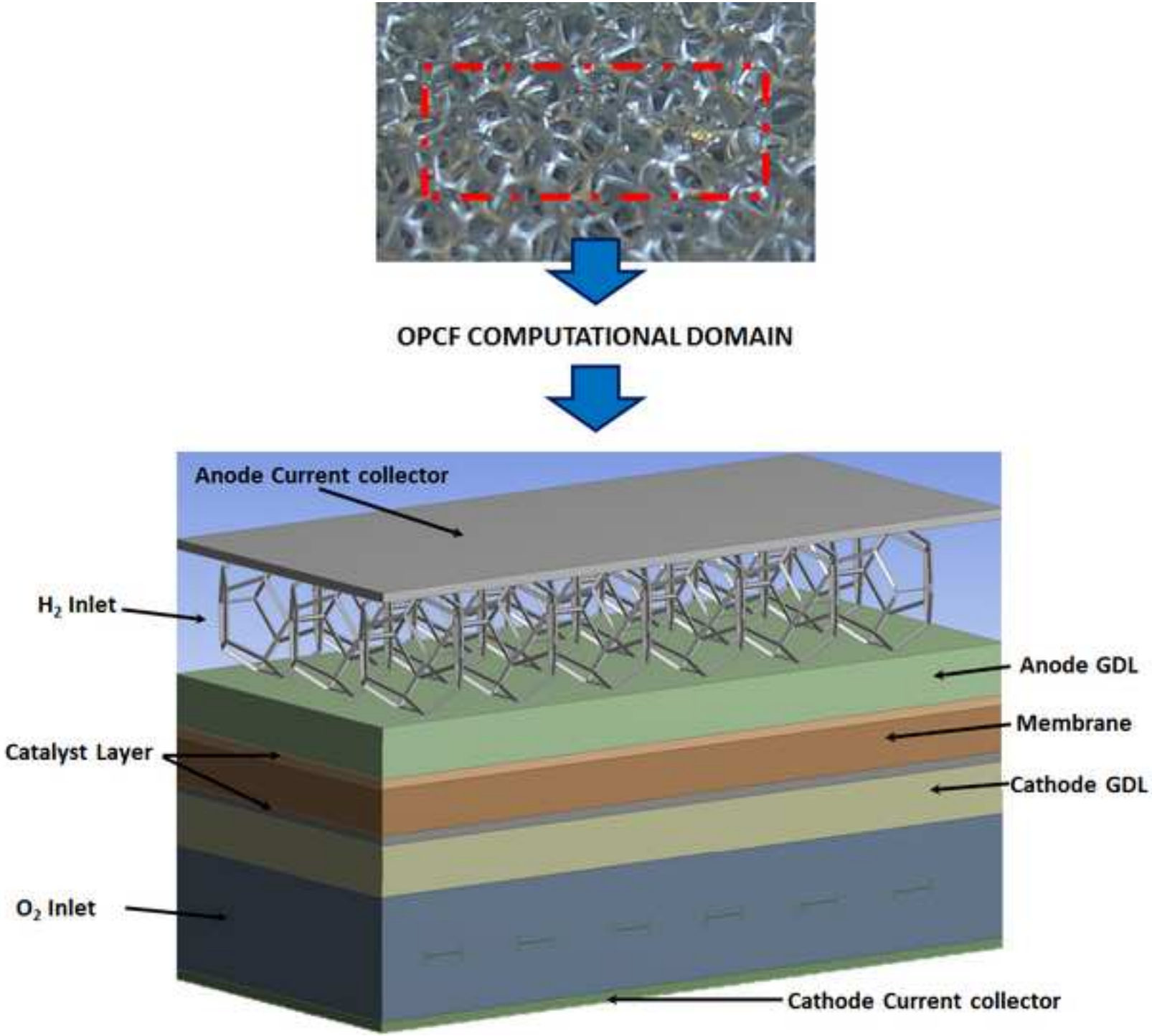

Figure 3
Click here to download high resolution image

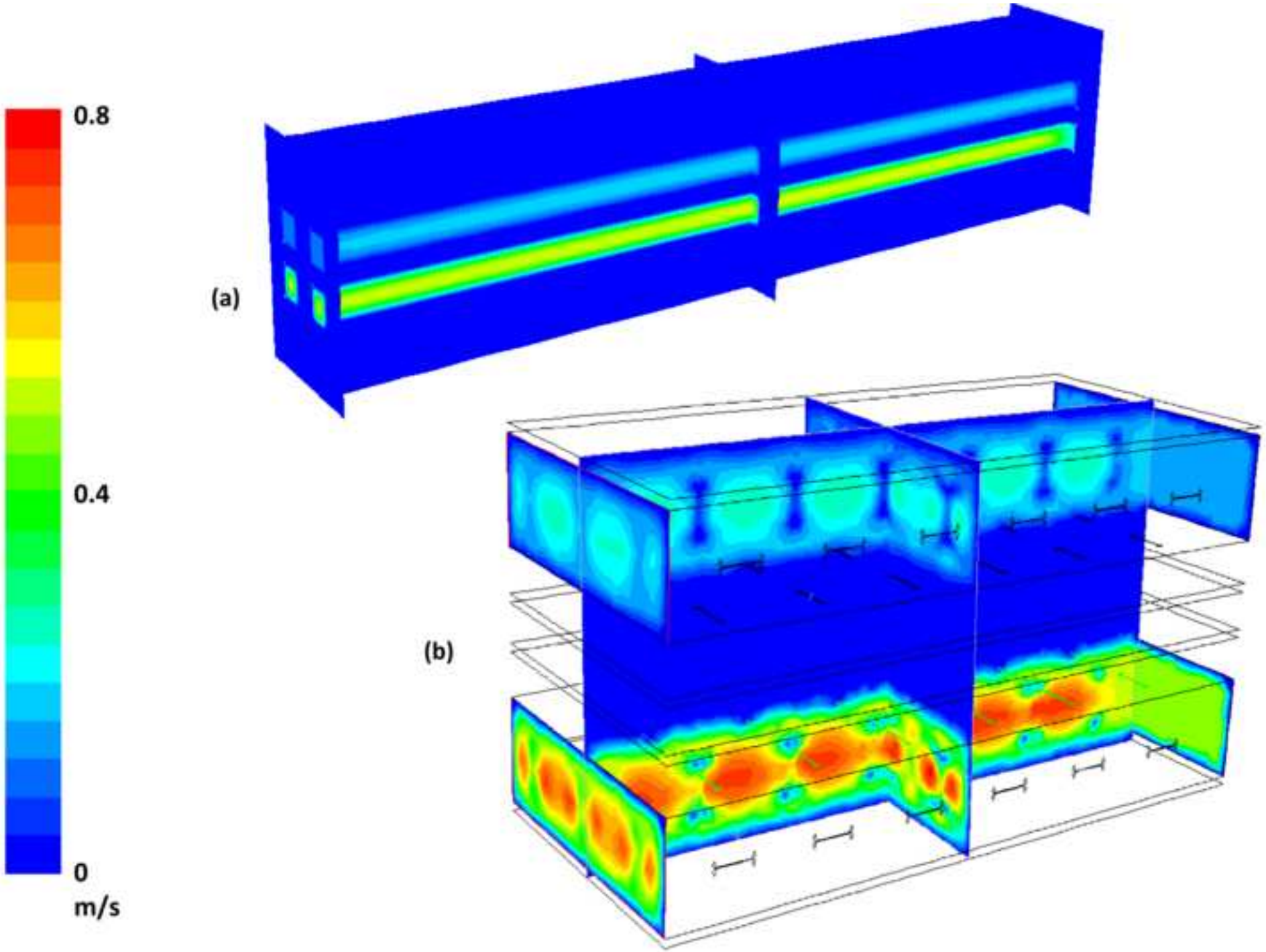

Figure 4

Click here to download high resolution image

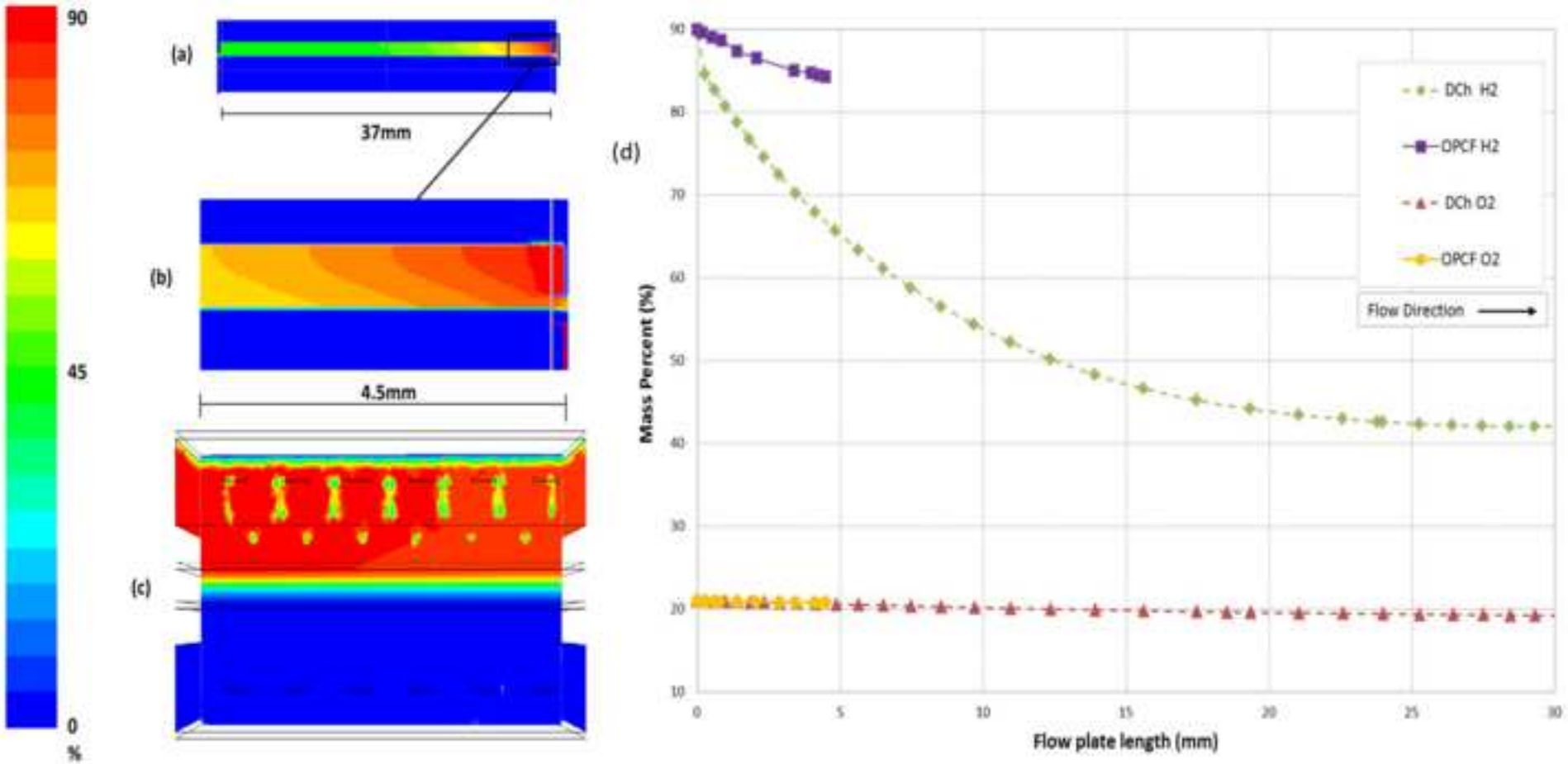

Figure 5

Click here to download high resolution image

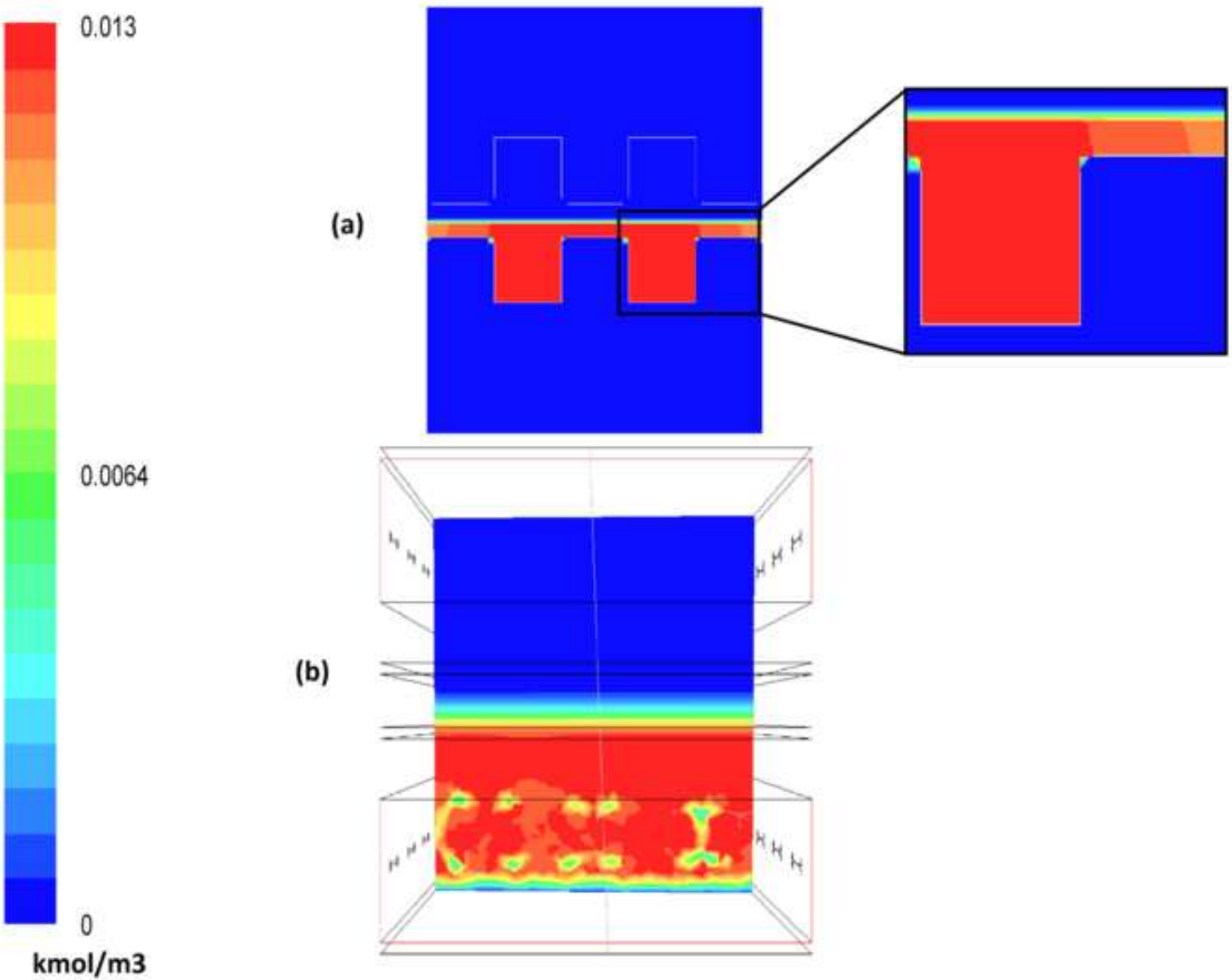

Figure 6

Click here to download high resolution image

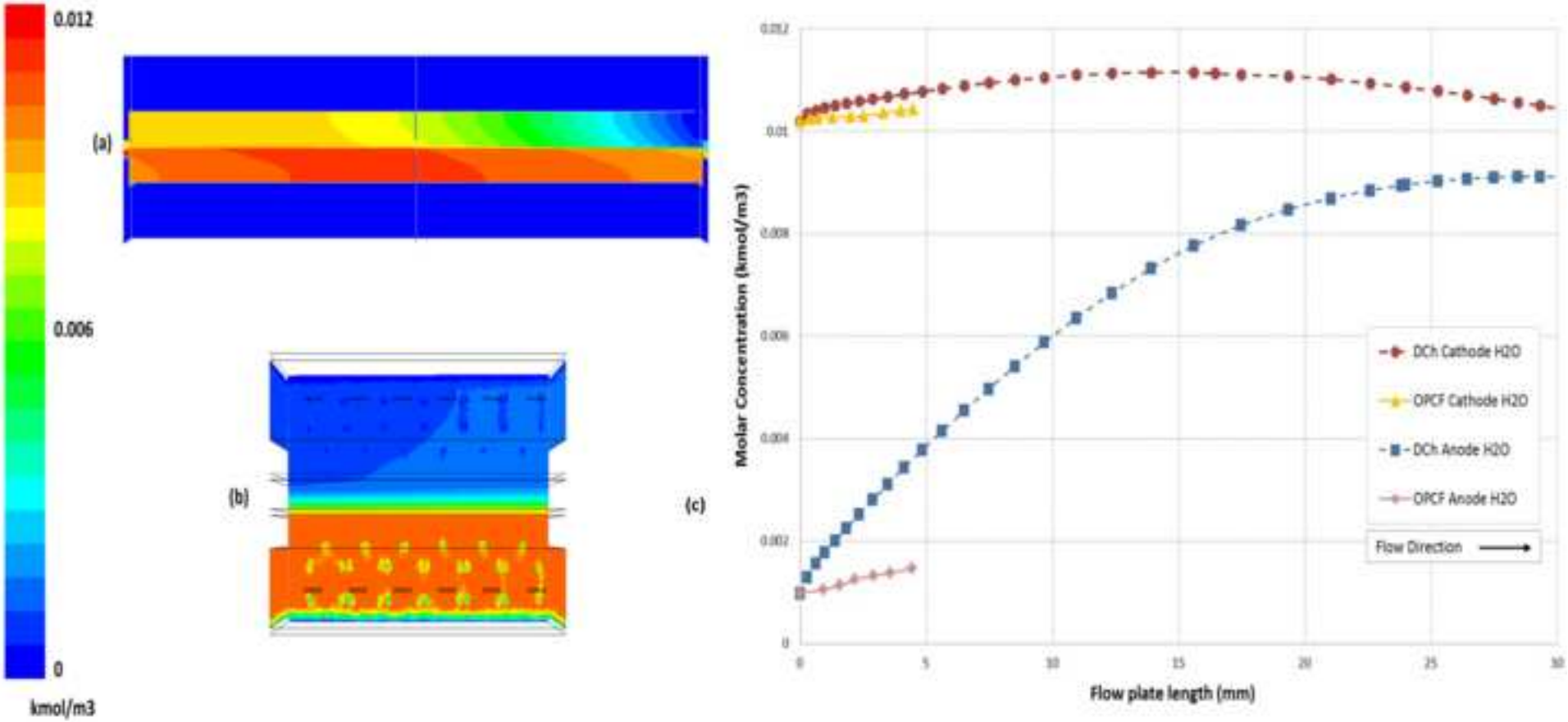

Figure 7

Click here to download high resolution image

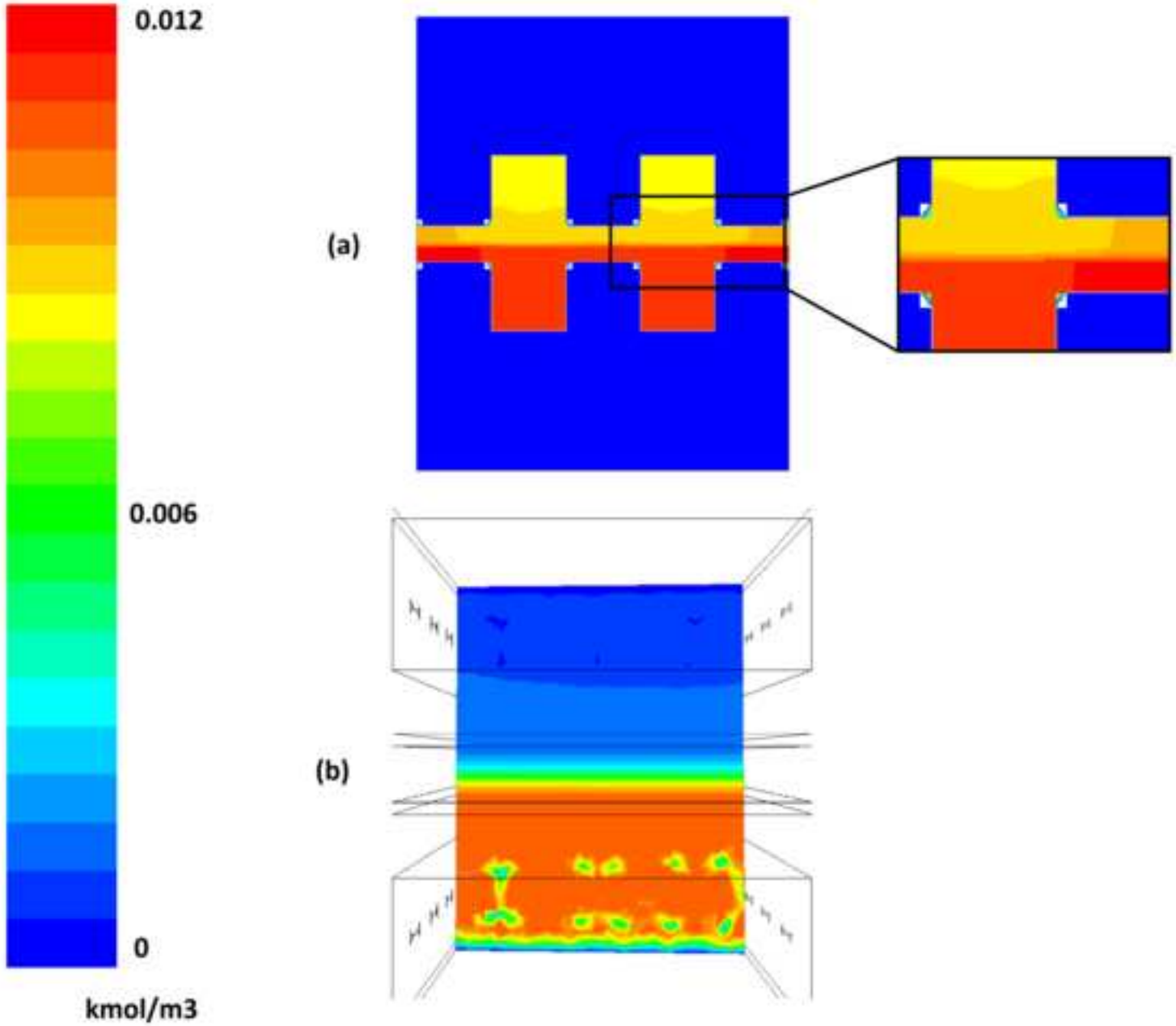

Figure 8

Click here to download high resolution image

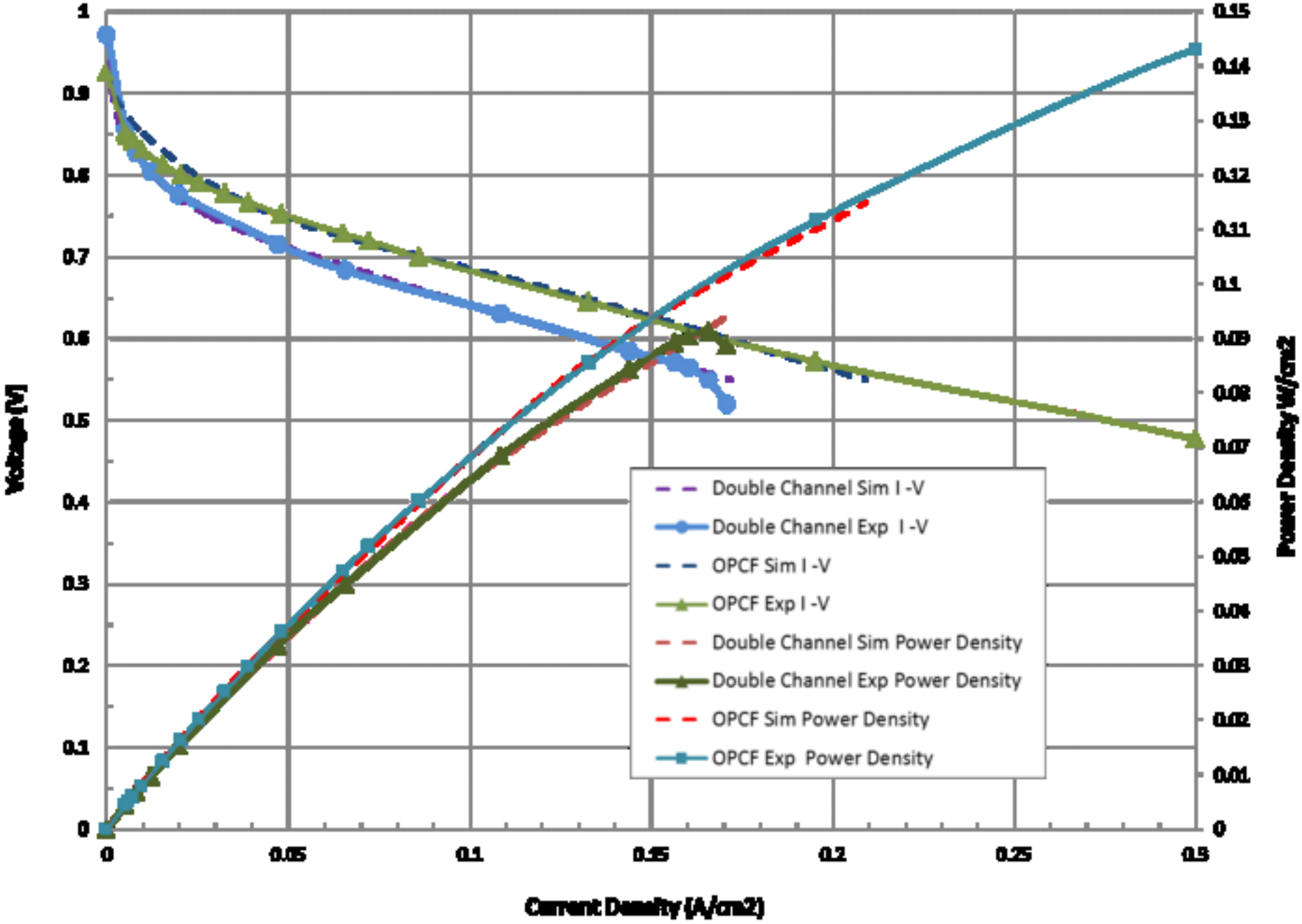

Table 1:

Zone	Description	Type	Notes
Anode current collector	**Conducts current**	**Solid**	**0 volts aluminium / graphite**
Anode flow channel	**Hydrogen gas flow**	**Fluid**	**Hydrogen & water vapour**
Anode gas diffusion layer	**Carbon layer**	**Fluid**	**Default GDL material**
Anode catalyst layer	**Platinum coating layer**	**Fluid**	**Default Pt catalyst material**
Membrane layer	**Active membrane**	**Fluid**	**Default membrane**
Cathode catalyst layer	**Platinum coating layer**	**Fluid**	**Default Pt catalyst material**
Cathode gas diffusion layer	**Carbon layer**	**Fluid**	**Default GDL material**
Cathode flow channel	**Air (oxygen) gas flow**	**Fluid**	**Oxygen, nitrogen & water vapour**
Cathode current collector	**Conducts current**	**Solid**	**Fixed voltage aluminium / graphite**

Table 2:

Parameter	Value	Units
Operating pressure	**2E+05**	**Pa**
Temperature	**60**	**°C**
Electrochemically active area	**OPCF 9.0 E-06** **DCh 19.25 E-06**	**m^2**
Anode Thickness	**5E-05**	**M**
Cathode Thickness	**5E-05**	**M**
Anode exchange current density	**10E+06**	**A/m^3**
Anode reference concentration	**1**	**$kmol/m^3$**
Anode concentration exponent	**0.5**	**-**
Anode exchange coefficient	**2**	**-**
Cathode exchange current density	**5E+04**	**A/m^3**
Cathode reference concentration	**1**	**$kmol/m^3$**
Cathode concentration exponent	**1**	**-**
Exchange coefficient	**2**	**-**
Diffusivity hydrogen	**6E-05**	**m^2/s**
Diffusivity oxygen	**3.5E-05**	**m^2/s**
Diffusivity water vapour	**6E-05**	**m^2/s**
Diffusivity other gases	**8E-05**	**m^2/s**
Multiphase saturation exponent	**2**	**(for pore blockage)**

Table 3:

PEM Fuel Cell model	**On**
Surface energy source	**On**
Disable CO electrochemistry	**Off**
Volumetric energy	**Off**
Solver type	**Pressure based**
Pressure	**standard**
Pressure-velocity coupling	**SIMPLE**
Formulation	**Implicit**
Time	**Steady**
Velocity formulation	**Absolute**
Gradient option	**Green gauss cell based**
Porous formulation	**Superficial velocity**
Energy equation	**On**
Viscous model	**Laminar**
Species sources	**On**
Species model	**Species transport**
Species options	**Diffusion energy source**
Mixture species	**O2 N2 H2O H2**

Table 4:

	Flow Plate	**Gas Diffusion Layer**	**Catalyst Layer**	**Polymer Electrolyte Membrane**
Material	**Aluminium 6061**	**Porous carbon**	**Pt carbon**	**Nafion 1110 [12]**
Porosity	**-**	**0.5**	**0.5**	**Nafion 1110 [12]**
Thickness (m)	**DCh 1E-3** **OPCF 6.2E-4**	**26E-5**	**5E-5**	**23E-5**

Table 5:

Parameter	Anode	Cathode
Inlet fluid	**Hydrogen**	**Air**
Inlet flow rate (ml/min)	**20**	**55**
Inlet pressure (gauge Pa)	**2E+05**	**2E+05**
Humidification (% at 55°C)	**80-90**	**80-90**
PEM fuel cell Temperature (°C)	**50-60**	**50-60**
Back Pressure (gauge Pa)	**0**	**0**

Tables

Figures